AGU PUBLICATIONS

Water Resources Research

RESEARCH ARTICLE
10.1002/2015WR017587

Key Points:
- A method to estimate the sensible heat flux, H, based on surface renewal, SR, is proposed, HSR
- HSR does not requires high-frequency measurements as input
- Because HSR involves the land surface temperature can be used in remote sensing

Correspondence to:
F. Castellví,
f-castellvi@macs.udl.cat

Citation:
Castellví, F., C. Cammalleri, G. Ciraolo, A. Maltese, and F. Rossi (2016), Daytime sensible heat flux estimation over heterogeneous surfaces using multitemporal land-surface temperature observations, *Water Resour. Res.*, *52*, 3457–3476, doi:10.1002/2015WR017587.

Received 22 MAY 2015
Accepted 4 APR 2016
Accepted article online 6 APR 2016
Published online 7 MAY 2016

Daytime sensible heat flux estimation over heterogeneous surfaces using multitemporal land-surface temperature observations

F. Castellví[1], C. Cammalleri[2], G. Ciraolo[3], A. Maltese[3], and F. Rossi[4]

[1]Department of Environment and Soil Sciences, University of Lleida, Lleida, Spain, [2]Joint Research Centre, European Commission, Ispra, Italy, [3]Department of Civil Engineering, Environmental, Aerospace, and Material (DICAM), Università degli Studi di Palermo, Palermo, Italy, [4]Institute of Biometeorology (IBIMET), Italian National Research Council, Bologna, Italy

Abstract Equations based on surface renewal (SR) analysis to estimate the sensible heat flux (H) require as input the mean ramp amplitude and period observed in the ramp-like pattern of the air temperature measured at high frequency. A SR-based method to estimate sensible heat flux ($H_{SR\text{-}LST}$) requiring only low-frequency measurements of the air temperature, horizontal mean wind speed, and land-surface temperature as input was derived and tested under unstable conditions over a heterogeneous canopy (olive grove). $H_{SR\text{-}LST}$ assumes that the mean ramp amplitude can be inferred from the difference between land-surface temperature and mean air temperature through a linear relationship and that the ramp frequency is related to a wind shear scale characteristic of the canopy flow. The land-surface temperature was retrieved by integrating in situ sensing measures of thermal infrared energy emitted by the surface. The performance of $H_{SR\text{-}LST}$ was analyzed against flux tower measurements collected at two heights (close to and well above the canopy top). Crucial parameters involved in $H_{SR\text{-}LST}$, which define the above mentioned linear relationship, were explained using the canopy height and the land surface temperature observed at sunrise and sunset. Although the olive grove can behave as either an isothermal or anisothermal surface, $H_{SR\text{-}LST}$ performed close to H measured using the eddy covariance and the Bowen ratio energy balance methods. Root mean square differences between $H_{SR\text{-}LST}$ and measured H were of about 55 W m^{-2}. Thus, by using multitemporal thermal acquisitions, $H_{SR\text{-}LST}$ appears to bypass inconsistency between land surface temperature and the mean aerodynamic temperature. The one-source bulk transfer formulation for estimating H performed reliable after calibration against the eddy covariance method. After calibration, the latter performed similar to the proposed SR-LST method.

1. Introduction

A reliable quantification of evapotranspiration (ET) fluxes is crucial in several hydrological and agro-meteorological applications, including drought monitoring and agricultural water management [e.g., *Allen et al*., 2005; *Anderson et al*., 2011; *Mu et al*., 2013]. To estimate ET at regional or larger scales, it is common to utilize modeling approaches rather than observations, mainly because sparse measurement networks are unable to capture the spatial variability of the moisture flux. Ideally, ET models should be able to perform robustly under a variety of conditions and to exploit readily available data sets.

A widely adopted class of methods for ET assessment is based on the use of land-surface temperature (LST) within the framework of surface energy balance (SEB) [*Norman et al*. 1995; *Bastiaanssen et al*. 1998; *Su*, 2000]. LST-based approaches commonly exploit a variety of remote sensing LST data [*Kalma et al*., 2008], ranging from images collected by satellite and airborne platforms to local records from in situ sensors. Overall, these methods have the common feature of adopting LST as a proxy variable that quantifies the effects of water availability on vegetated land.

In LST-based applications, the latent heat flux (λET) is often determined as a residual of a simplified SEB, in which the available energy at the surface, given by the difference between the net radiation (R_n) and the soil heat flux (G), is partitioned between λET and sensible heat flux (H) [e.g., *Allen et al*., 2005]. Even if LST plays an important role in determining the upwelling long-wave component of R_n as well as surface

boundary conditions of the soil temperature profile to estimate G [*Crago and Qualls*, 2014], it is largely accepted that its main role in residual SEB models is in the modeling of H fluxes.

Over homogeneous surfaces (including either full canopies or bare soils), SEB can be applied under the assumption of isothermal surfaces; in this simple case, the aerodynamic temperature (T_0) and the LST have often been assumed as identical for operational purposes [*Norman and Becker*, 1995] and the one-source bulk transfer formulation based on Monin-Obukhov Similarity Theory (MOST) has been used to estimate H starting from the temperature gradient between the land surface and the air temperature at a certain height (T_Z). Integration of the temperature gradient involves the parameter kB^{-1} which often has been presumed fairly constant. However, for more than five decades the parameter kB^{-1} has been a matter of basic research because its behavior and parameterization beyond neutral cases is not well understood [*Kustas et al*., 1989; *Castellví et al*., 2014].

In most operational applications, however, the hypothesis of homogeneous surface is violated, even when high resolution thermal data are used; this is particularly true over agricultural landscapes characterized by fragmented crops. Heterogeneous canopies generally behave as anisothermal surfaces; therefore, LST and T_0 are in general not equal and their relationship is ill-defined, as are the surface roughness parameters [*Blyth and Dolman*, 1995; *Haverd et al*., 2010]. Empirical approaches have been proposed to correct LST or roughness parameterization to allow estimating H from LST observations acquired over heterogeneous surfaces [*Boulet et al*., 2012; *Chehbouni et al*., 1996]; however, these approaches have limited applicability due to their empirical nature.

Heterogeneous crops are better described by the two-source bulk transfer modeling approach, which is preferable to the one-source formulation for these cases. In the two-source approaches, the total H fluxes above the canopy are quantified by integrating the contributions coming from soil and vegetation and resolving analytically the relation between LST and T_0 based on the fraction occupied by each source, as in the two-source energy balance (TSEB) model proposed by *Norman et al*. [1995]. Although TSEB removes the need for empirical correction factors, some assumptions are required to obtain a closed form for solving the system of equations (e.g., use of a simplified formulation for vegetation transpiration [*Priestley and Taylor*, 1972]) and, in general, a higher number of parameters and a more complex parameterization are needed.

Independently from the adopted modeling framework (i.e., one- or two- source), the accuracy of H estimates is directly affected by the reliability of LST observations, which is a function of calibration and correction procedure of the raw thermal data [e.g., *Jacob et al*., 2004]. While some problems are limited only to satellite and airborne data, others are common to all thermal measurements (i.e., including in situ sensing). Satellite LST estimates are commonly affected by atmospheric emission, absorption, and scattering that need to be removed from the observed signal; other common corrections of all the thermal data are related to the divergence of actual surface emissivity from the ideal black body [*Schmugge*, 2006]. Despite all the efforts to develop algorithms suitable for correcting atmospheric influence on thermal remote sensing data [e.g., *Berk et al*., 1998; *Wan and Dozier*, 1996; *Gillespie et al*., 1998] and accurately estimating surface emissivity [e.g., *Dash et al*., 2002; *Schmugge et al*., 2001], the highest LST accuracy is generally on the order of 1–1.5 K [*Gillespie et al*., 1998; *Jiménez-Munõz and Sobrino*, 2007; *Morillas et al*., 2013]. This accuracy is often comparable with the magnitude of the temperature gradient driving H [*Norman et al*., 2000]; thus, the absolute accuracy of LST becomes a relevant source of uncertainty in SEB approaches [*Liu et al*., 2007], and the adoption of a method to minimize inconsistency between LST and T_Z data is a crucial step for a reliable H estimation.

A solution to this problem, based on a time-differential application of TSEB within the Atmosphere-Land Exchange Inverse (ALEXI) model, was proposed by *Anderson et al*. [1997]; however, this approach requires additional inputs, such as the availability of an early morning atmospheric temperature profile. A simplified version of this approach was proposed by *Norman et al*. [2000], the dual-temperature-difference (DTD) method, which exploits the change in air temperature observations at two times of the day. In *Guzinski et al*. [2013] this method showed some potential related to the use of day-night LST observations.

Surface renewal SR analysis (pioneered by *Paw et al*. [1995]) for estimating the flux of a scalar is grounded on the scalar conservation equation and assumes that the turbulent exchange on any scalar is driven by the regular replacement of a parcel of air in contact with the sources in the surface where the exchange occurs. SR analysis is an alternative to MOST-based formulation because it is based on different principles and

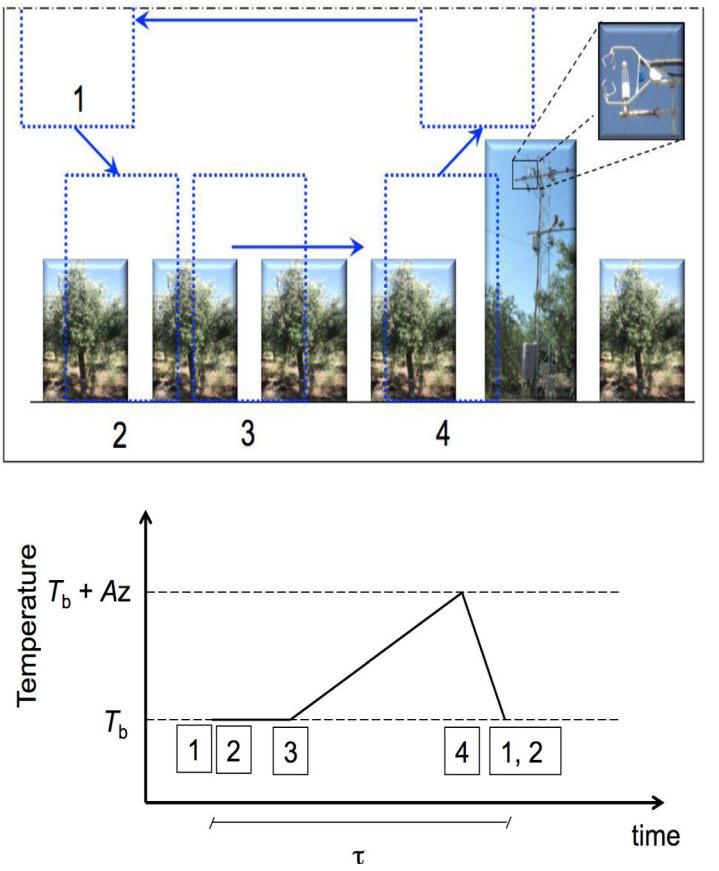

Figure 1. (top) Cartoon of a parcel of air illustrating the renewal process. (bottom) For unstable conditions, ideal time course of the air temperature measured at Z for the positions shown in the top plot (ramp model). A parcel of air with temperature T_b traveling above the surface (1) suddenly descends to the surface (2) and, after a quiescent period (3), it gradually warms (4), until it is replaced by another parcel of air. A_Z is the ramp amplitude and τ is the total ramp duration. The ramp model assumes that the parcel of air is uniformly heated.

operates in both the roughness and inertial sublayers. From a pseudo-Lagrangian point of view, the Figure 1 shows the key idea of the SR method for estimating H. In the top plot in Figure 1 is sketched the SR process by assuming that a coherent structure is capable to explain most of H [*Gao et al.*, 1989; *Paw et al.*, 1995; *Hongyan et al.*, 2004]; a parcel of air, originally traveling above the surface with a temperature T_b, suddenly sweeps down to the surface. Therefore, it remains in contact with the surface for a given period (ramp duration) which includes three phases: after a quiescent phase during which the temperature of the parcel of air is still close to that observed at the original height (i.e., T_b), the parcel gradually warms (warming phase) until, by continuity, it is replaced by another parcel of air coming from aloft (ejection phase). The parcel of air ejected represents an injection of heat into the atmosphere. For a given period of time (e.g., half-hour), several ejections take place, which explains the ramp-like pattern observed in the time series of the air temperature measured at high frequency. Figure 1 (bottom) shows a ramp model, which is an ideal time course of the temperature of the parcel of air along the total ramp duration. The ramp model assumes that the parcel of air is uniformly heated. In practice, because it is not uniformly heated, within the volume of the parcel there are smaller eddies attached and the temperature of the air is measured at a fixed point, the actual ramp-like pattern differs from that shown in the ramp model. The analysis consists in applying numerical methods to the air temperature measured at high frequency to obtain the mean ramp amplitude (A) and total period (τ) shown in the ramp model, such as Fourier transform, filtering techniques, wavelet transformation, pseudo-wavelet and closely related principal component analysis methods, and analysis of structure functions of different order in conjunction with the proposal of ramp models [*Van Atta*, 1977; *Gao et al.*, 1989; *Shaw et al.*, 1989; *Berkooz et al.*, 1993; *Qiu et al.*, 1995; *Paw et al.*, 1995; *Katul et al.*, 1996; *Chen et al.*, 1997a; *Paw et al.*, 2005; *Shapland et al.*, 2012a]. The latter methodology has been mostly used in SR analysis because it is objective (i.e., there is no need to select a priori specific filters and functions) [*Paw et al.*, 2005].

Fine wire thermocouples often broke in field conditions. Therefore, it is desirable to use robust (i.e., thicker) thermocouples for an operational application of the SR analysis. Because the ramp model shown in Figure 1 requires determination of three phases (quiescence, warming and ejection), other ramp models have been proposed such as the ones proposed by *Chen et al.* [1997a], which neglects the quiescent phase, and by *Van Atta* [1977], which accounts for the quiescent phase but neglects the ejection phase. The latter has been the most used ramp model because the total ramp period and amplitude can be estimated measuring the air temperature at frequencies of about 10 Hz [*Chen et al.*, 1997a; *Paw et al.*, 2005]. However, the *Chen*

et al.'s [1997a] ramp model, which better describes the actual structure functions, requires measurements taken at frequencies of about 20 Hz.

In the following, the mean ramp amplitude determined at a height Z above the ground is denoted as A_z while the ramp period is still denoted as τ to clarify that the former is dependent on the measurement height while the latter remains fairly constant with height [*Paw et al.*, 2005].

Castellví et al. [2014] proposed to linearly relate $(\mathrm{LST} - T_Z)$ and A_Z, showing that a linear relationship holds for a wide range of atmospheric stability conditions over dense, short, irrigated grass. Therefore, it was possible to derive SR-based equations for estimating H over a homogeneous canopy requiring measurements taken at low frequency as input.

Noteworthy that the SR-flux approaches that do not require the ramp period as input have performed closely to the Eddy Correlation (EC) method over both homogeneous and heterogeneous canopies [e.g., *Castellví et al.*, 2002; *Castellví*, 2004; *Castellví et al.*, 2014]. It is, therefore, of interest to know if a linear relationship between $(\mathrm{LST} - T_Z)$ and A_Z applies also for a heterogeneous canopy and if the two coefficients involved (slope and intercept) can be estimated using readily available measurements as input. The latter is crucial for deriving an operational SR-based equation that would offer an alternative approach to the classical bulk transfer formulation for possible remote sensing applications.

An experiment was conducted in an olive orchard during spring and summer in Sicily (Italy) to investigate the relationship between $(\mathrm{LST} - T_Z)$ and A_Z over a heterogeneous surface under unstable conditions, because it is of major interest for operational remote sensing-based applications. Provided that the relationship between $(\mathrm{LST} - T_Z)$ and A_Z can be explained, it allows avoiding both the discrepancy between LST and T_0 in heterogeneous canopies and the likely inconsistency between LST and T_Z data calibration. It is anticipated that the linear relationship between $(\mathrm{LST} - T_Z)$ and A_Z holds and that the two coefficients involved can be explained by means of multitemporal acquisitions of LST and the canopy height. Hence, a self-calibrated SR-based approach useful in the framework of remote sensing for estimating H was proposed minimizing the uncertainty involved in the parameter kB^{-1} (only required at neutral conditions). The approach has been tested using as input thermal data collected in situ to maximize accuracy and control on the model inputs. The sensible heat flux was estimated at two heights using measurements close to and well above the canopy top.

2. Theory

In SR analysis for estimating the sensible heat flux, by assuming a uniformly heated parcel of air which has a volume (V) per unit surface area (S) equaling the measurement height above the ground (i.e., $V/S=Z$), the quantity $Z\rho C_p A_Z$ (where ρ and C_p are the air density and the isobaric specific heat, respectively) is the heat exchanged per unit surface across Z. Because the inverse of the ramp period is the frequency of injections of heat into the atmosphere, the earlier SR method estimates the sensible heat flux (H_{SR_1}) as [*Paw et al.*, 1995]:

$$H_{SR\_1} = \alpha_Z Z \rho C_p \frac{A_Z}{\tau}, \tag{1}$$

where subscript 1 denotes the first SR equation proposed and α_Z is a parameter that accounts for the uneven heating within the air parcel. The parameter α_Z has been determined using linear regression analysis comparing the H measured using the EC method against $Z\rho C_p \frac{A_Z}{\tau}$ [*Snyder et al.*, 1996]. After calibration of parameter α_Z, equation (1) has been used for estimating H using the air temperature measured at high frequency, as well as the latent heat flux as a residual of the surface energy balance [*Anderson et al.*, 2003; *Drexler et al.*, 2008; *Mengistu and Savage*, 2010; *Moratiel and Martínez-Cob*, 2012]. Some experiments have shown that under near neutral conditions α_Z is approximately 0.5. In general, and regardless of the ramp model used, α_Z depends on the measurement height and the stability conditions [*Paw et al.*, 1995; *Katul et al.*, 1996; *Snyder et al.*, 1996; *Castellví*, 2004; *Castellví and Snyder*, 2009; *Shapland et al.*, 2012b]. Two expressions have been derived to explain the variability of parameter α_Z, the first requires as input the horizontal wind speed [*Castellví*, 2004] and the second the temperature gradient [*Castellví*, 2013]. Therefore, SR-based flux equations were obtained exempt of calibration [*Castellví et al.*, 2008; *Castellví and Snyder*, 2009, 2010;

Suvočarev et al., 2014]. One of the latter SR-flux equations, described next (equation (2)), is convenient for the purpose of this study because the measurements required as input can be taken at one height.

Implementing the time course of the air temperature described in the ramp model of *Chen et al.* [1997a] within the one-dimensional diffusion equation, the sensible heat flux can be estimated involving the mean ramp amplitude and period (H_{SR}) as [*Castellví*, 2004, 2013]:

$$H_{SR}=\rho C_p\sqrt{\frac{kzu_*\gamma\varphi^{-1}_{h(z/L)}}{\pi\tau}}A_Z, \tag{2}$$

where k is the von-Kármán constant, z is the measurement height above the zero-plane displacement (d), thus $z=Z-d$, u_* is the friction velocity, L is the Obukhov length, $\phi_{h(z/L)}$ is the stability correction function for heat transfer and γ is the enhancement correction factor that corrects the departure of $\varphi^{-1}_{h(z/L)}$ in the roughness sublayer [*Cellier and Brunet*, 1992; *Mölder et al.*, 1999]; $\gamma=\begin{cases}\frac{z^*}{z} & h\le z\le z^*\\ 1 & z>z^*\end{cases}$ where z^* is the height of the roughness sublayer above d. Thus, $z^*=Z^*-d$ where Z^* is the height of the roughness sublayer above the ground.

2.1. Estimating H_{SR} Without Requiring the Ramp Period as Input

Because coherent motions (Figure 1) are mainly shear-driven, they explain most of momentum transferred to the ground. Therefore, the semiempirical relationships $\frac{1}{\tau}=\lambda_1\frac{u_h}{h}$ and $u_h=\lambda_2 u_*$ were analyzed over different canopies [*Antonia et al.*, 1979; *Gao et al.*, 1989; *Paw et al.*, 1992; *Shaw et al.*, 1995; *Raupach et al.*, 1996; *Graefe*, 2004; *Finnigan et al.*, 2009], where u_h is the horizontal mean wind speed at the canopy top, h is the canopy height, $\frac{u_h}{h}$ is a wind shear scale characteristic of the canopy flow, and λ_1 and λ_2 are two coefficients. Therefore, the following relationship holds:

$$\frac{1}{\tau u_*}=\frac{\lambda_h}{h}, \tag{3}$$

where λ_h is a coefficient, $\lambda_h=\lambda_1\lambda_2$. Combining equations (2) and (3), the sensible heat flux can be expressed without involving the ramp period:

$$H_{SR}=\rho C_p\sqrt{\frac{\lambda_h k}{\pi}\frac{z}{h}\gamma\varphi^{-1}_{h(z/L)}}u_*A_Z. \tag{4}$$

2.2. Estimating H_{SR} Involving the Land Surface Temperature

Regardless of the surface, here it is assumed that a linear relationship between A_Z and the difference between LST and T_Z, holds:

$$\mathrm{LST}-T_Z=a+s_ZA_Z, \tag{5}$$

where a and s_Z are the intercept and the slope of the linear relationship, respectively. Equation (5) states a relationship between two temperature surface scales that are used in the bulk transfer formulation for applications in remote sensing, $\mathrm{LST}-T_Z$, and the scale used in SR analysis, A_Z. Appendix A shows that the intercept a corrects for differences between the aerodynamic temperature and LST and that the slope may be interpreted as the ratio between the vertical surface velocity scale for heat transfer predicted by MOST and by SR analysis. Equation (5) was first analyzed in the inertial sublayer over a homogeneous canopy [*Castellví et al.*, 2014]. Combining equations (4) and (5) allows expressing the following SR-flux expression for estimating the sensible heat flux involving LST ($H_{SR\text{-}LST}$):

$$H_{SR\text{-}LST}=\rho C_p\sqrt{\frac{\lambda_h k}{\pi}\frac{z}{h}\gamma\varphi^{-1}_{h(z/L)}}u_*\frac{[LST-(T_Z-a_Z)]}{s_Z}. \tag{6}$$

In the earlier SR-flux equations high-frequency measurements of air temperature are required as input. However, equation (6) suits for the purpose of this study provided that standard low frequency measurements are required as input for estimating the coefficient λ_h, the roughness sublayer depth and parameters a and s_Z (as described in appendix A). Parameterizations based on the mean wind profile can be used to estimate u_* (described in appendix B).

For estimating H over bare soils it is convenient to express equation (3) as described in equation (A1): $\frac{1}{\tau u_*} = \frac{\lambda_h}{h} = \frac{\lambda_Z}{Z}$. The latter, allows rewriting equation (4) as:

$$H_{SR} = \rho C_p k \delta \varphi_{h(z/L)}^{-1} u_* A_Z \text{ where } \delta = \sqrt{\frac{\lambda_z}{k\pi}\varphi_{h(z/L)}}. \quad (7)$$

Though using an alternative dimensional analysis, equation (7) was originally proposed in *Castellví et al.* [2002] with δ a coefficient to be calibrated. Under near-neutral and unstable conditions, the parameter δ was found approximately 0.5 for different canopies [*Castellví et al.*, 2002; *Castellví*, 2004]. However, it has not been determined over bare soils. Provided that the coefficient δ is known, the approach for estimating H obtained combining equations (5), (7), and (A10) best suits for bare soils because the canopy height is not an input. Under convective conditions, the coefficient λ_Z was determined for a bare soil taking measurements at $Z = 0.03$ m, $\lambda_Z = 0.4$ [*Chen et al.*, 1997b]. Therefore, the coefficient δ estimated from equation (7) is $\delta = 0.56$ because for this case (i.e., z/L is close to zero) $\varphi_{h(z/L)}$ can be set to $\varphi_{h(z/L)} = 1$. Regardless, further research is required to determine the coefficient δ over different bare soils, wide range of stability conditions and measurement heights.

2.3. Estimation of Parameters a and s_Z for Homogeneous and Moderately Heterogeneous Canopies

In this study it is assumed that multitemporal LST observations are available over a heterogeneous canopy, which will allow estimating a at near-neutral conditions, such as around sunrise and sunset. It is assumed that a values remain fairly constant for a given period during the day. Therefore, the a value determined at sunrise (sunset) will be used in equation (5) for the samples collected during the morning (afternoon). The parameter s_Z is assumed to remain fairly constant under near-neutral and unstable cases; therefore, s_Z was estimated under near neutral conditions. According to these two assumptions, the following approaches are proposed as input in equation (6) for parameters a and s_Z (equations (A8) and (A9), respectively):

$$a_{(z/L=0)} = LST_{(z/L=0)} - T_{Z(z/L=0)}, \quad (8)$$

and

$$s_Z = \left(\frac{\lambda_h}{2k}\frac{Z}{h}\right)\left(\ln\left(\frac{z}{z_{0m}}\right)+2\right) \text{ with } \lambda_h = 0.55. \quad (9)$$

2.4. Estimation of $h_{SR\text{-}LST}$ Under Near-Neutral and Unstable Conditions

Combining equations (6), (8), (9), and (A2) the following expression for $H_{SR\text{-}LST}$ is proposed for homogeneous and moderately heterogeneous surfaces:

$$H_{SR-LST} = \rho\, C_p \frac{\left[(Z-d)h\,\gamma\varphi_{h(z/L)}^{-1}\right]^{1/2}}{Z} \frac{k u_* \left[LST - \left(T_Z + a_{(z/L=0)}\right)\right]}{\left(\ln\left(\frac{Z-d}{z_{0m}}\right)+2\right)} \quad \text{with} \begin{cases} \gamma = 1 & Z \geq Z^* \\ \gamma = \dfrac{Z^*-d}{Z-d} & Z < Z^* \\ Z^* - d = 1.4\,h & \\ \varphi_{h(z/L)} = \left(1 - 16\dfrac{Z-d}{L}\right)^{-1/2} & \end{cases} . \quad (10)$$

With regard to the earlier SR analysis applications, equation (10) opens a new SR-framework because H can be estimated without measurements taken at high frequency and suits for thermal remote sensing applications. In relation to the traditional bulk transfer formulations, such as the one-source (described in appendix A), equation (10) allows operating in the roughness sublayer. The latter allows avoiding installation of tall masts for tall canopies, which is a useful feature when the fetch is limited forcing deployment of instrumentation below the inertial sublayer.

3. Materials and Methods

3.1. The Field Experiment

The experimental campaign was conducted in an olive orchard in Castelvetrano (37°38′40″N, 12°50′47″E and 122 m asl) (Figure 2).

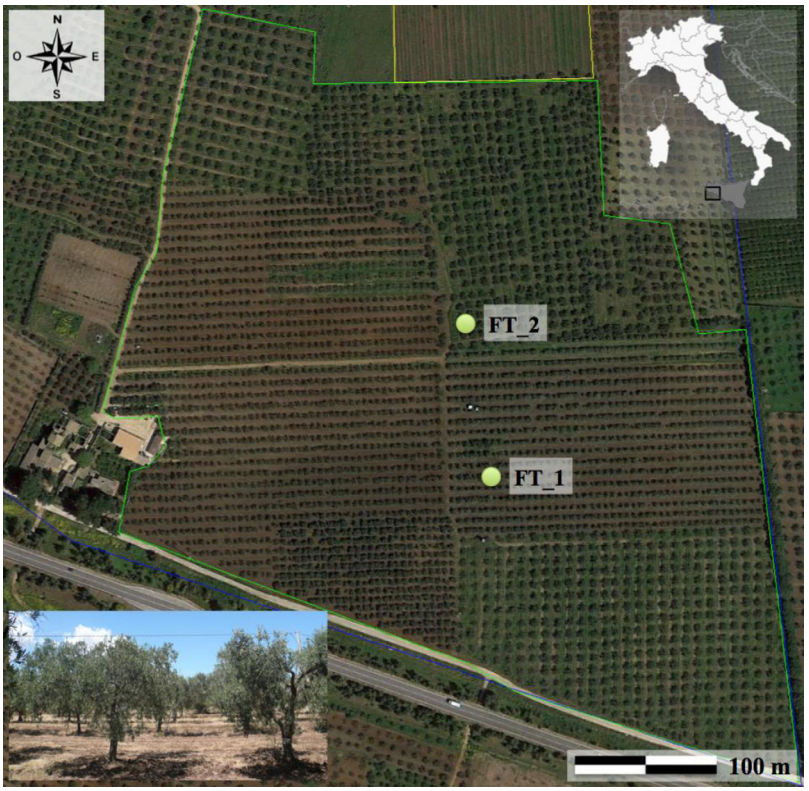

Figure 2. Orthophoto of the study area. Dots highlight the position of the two flux tower installations: FT_1 and FT_2. A panoramic view of the groove is included (bottom left).

The site is part of the CARBOITALY network within the European CARBOEUROPE framework; both site and climate are fully described in *Nardino et al*. [2013]. The olive orchard (11 ha, partly drip and partly sprinkler irrigated, and without understories during spring and summer) had four groves; each grove had slightly different characteristics (tree age, canopy height, planting density, and fraction of exposed soil (f_s)).

Data were collected by two flux tower installations, FT_1 (Flux Tower managed by the University of Palermo) and FT_2 (CARBOITALY flux site) (Figure 2) and several pictures of the experiments are available in *Cammalleri* [2011]. In FT_1 a 6 m mast was erected in 2010. The grove surrounding the tower was drip irrigated and characterized by $h = 3.3$ m and $f_s = 0.31$. A three-dimensional sonic anemometer (CSAT-3D, Campbell Sci., USA), a thermocouple (FW005, Campbell Sci., USA), and an open path infrared absorption gas analyzer (Li7500, LiCor Inc., USA) were deployed at $Z = 5.6$ m, both operating at a frequency of 20 Hz; raw data were stored in a datalogger (CR5000, Campbell Sci., USA). The four main components of R_n were measured using a CNR1 net radiometer (Kipp and Zonen) deployed at $Z = 4.5$ m. Two flux plates (HFP01, Campbell Sci., USA), one below the canopy and another within the row, were installed at a depth of 10 cm, and the probes measuring the soil temperature (Campbell Sci., Logan, UT, USA) were buried at 8 and 3 cm below ground level. In addition, two cables were set to hold two IRTS-P sensors (Campbell Sci. and Apogee Instruments, Inc.) to measure the half-hourly radiometric temperatures of the soil (TIR_s) and canopy (TIR_c). Half-hourly horizontal wind speed and direction were measured at $Z = 5.6$ m using a wind monitor (RM Young 05103); half-hourly air temperature and relative humidity were measured at the same height using an HMP45C probe (Vaisala Inc.).

FT_2 has been operating since 2006, and the grove surrounding this tower was characterized by $h = 3.3$ m and $f_s = 0.35$. Instrumentation deployed at $Z = 8$ m includes an EC unit (CSAT-3D and LiCor 7500 operating at 10 Hz), a net radiometer (NR Lite, Campbell Sci., USA), a wind monitor (RM Young 05103), and a thermo-hygrometer (HMP45C probe, Vaisala Inc.). Analogous to FT_1, the instrumentation to measure the soil heat flux was placed at two locations (one below the canopy and the other in a row).

3.2. Data Sets and Preprocessing

The analysis was performed on data sets collected at both towers from 15 April to 2 September 2010. Given that LST was not available at FT_2, the LST determined at FT_1 was assumed to hold at FT_2 because the groves were similar. Regardless, it is of interest to evaluate the impact on the H estimates arising from uncertainty in LST.

The half-hourly LST was obtained using the long-wave radiation measured at FT_1 accounting for the downwelling component (in the thermal part of the spectrum) reflected by the surface as follows:

$$LST=\left[\frac{R_{lu}-(1-\varepsilon_0)R_{ld}}{\sigma\varepsilon_0}\right]^{1/4}, \tag{11}$$

where R_{lu} and R_{ld} are the upwelling and downwelling long-wave radiation, respectively, σ is the Stefan-Boltzmann constant [*Brutsaert*, 1982], and ε_0 is the surface emissivity determined as [*Valor and Caselles*, 2005]:

$$\varepsilon_0=\varepsilon_v(1-f_s)+\varepsilon_s f_s(1.74f_s-0.74)+1.7372f_s(1-f_s), \tag{12}$$

with canopy and soil emissivity values set to $\varepsilon_v = 0.97$ and $\varepsilon_s = 0.93$. These are values commonly used for broad-band measurements [*Ogawa et al*., 2002]. Particularly, the soil surface emissivity refers to a dry soil since this is the most common condition in the experiment. During the sampling campaign, the effects of understories on ε_s were assumed negligible.

The mean ramp amplitude was determined using the *Chen et al*. [1997a] ramp model using half-hour air temperature traces. The EC data were processed following the standard EUROFLUX guidelines [*Aubinet et al*., 2000], and the soil heat flux was determined as described in *Fuchs and Tanner* [1967], and closure of the surface energy balance was checked. Regardless of the installation, on average 15% of the available energy was not explained by the EC fluxes, a closure consistent with that previously observed at FT_2 between 2006 and 2008 [*Nardino et al*., 2013]. Thus, the closure is within the range reported in the literature over other crop systems and forest [*Goulden et al*., 1996, *Aubinet et al*., 2000; *Wilson et al*., 2002; *Teixeira et al*., 2008; *Castellví et al*., 2012]. Because modeling approaches are commonly based on a perfect closure of SEB, the energy budget was forced at both sites to determine H using the Bowen ratio-energy balance (BREB) method [*Twine et al*., 2000]. The Bowen ratio, BR, defined as $BR=H/\lambda ET$ was determined using the EC method. Both the EC method (H_{EC}) and the BREB method (H_{BREB}) were used as reference values to analyze the performance of $H_{SR\text{-}LST}$. The references H_{EC} and H_{BREB} were compared, and the root mean square difference (RMSD) was 62 and 53 W m^{-2} at FT_1 and FT_2, respectively. The RMSD was set as a benchmark of uncertainty for the successive analyses.

3.3. Testing the Relationship Between A_Z and (LST − T_Z) at FT_1

Sinceequation (5) was studied and verified over homogeneous canopies only, it ensures neither the reliability of this relationship nor the robustness of parameters a and s_Z over heterogeneous canopies. The variability of a and s_Z was tested at FT_1 because A_Z and TIR_s/TIR_c were only available at this installation.

To test equation (5) the entire database was divided into six data sets, each had approximately 20 days, with filenames that corresponded to the date (*ddmmyy*) of the ending day. Data sets formed with about 2 weeks of data seemed, in general, appropriate because this schedule simulates the Landsat overpass frequency. The data sets were labeled as isothermal when $\Delta TIR=\overline{TIR_s-TIR_c} \leq 3K$ and anisothermal otherwise. In a wind tunnel experiment, differences much smaller than 3K between the *ground* (plate) and the top of a heterogeneous *canopy* (displaced ellipsoidal light globes) were considered to simulate a two-layer heat-source vertical distribution under near-neutral conditions [*Haverd et al*., 2010]. Regardless of the threshold, this classification is merely a formality because the goal for routine applications is to apply equation (10) regardless of the thermal behavior of the surface (i.e., the absolute difference between the average values TIR_s and TIR_c (ΔTIR) is rarely available). The classification was only used to check if any pattern existed between the temporal variability of parameters a and s_Z and the behavior of the surface.

For each data set, two mean a values were estimated at neutral conditions, one at sunrise (a_{am}) and the other at sunset (a_{pm}) taking the mean of (LST − T_Z) sampled at sunrise and at sunset, respectively, because for moderate measurement heights the air temperature is close to the aerodynamic temperature [*Brutsaert*,

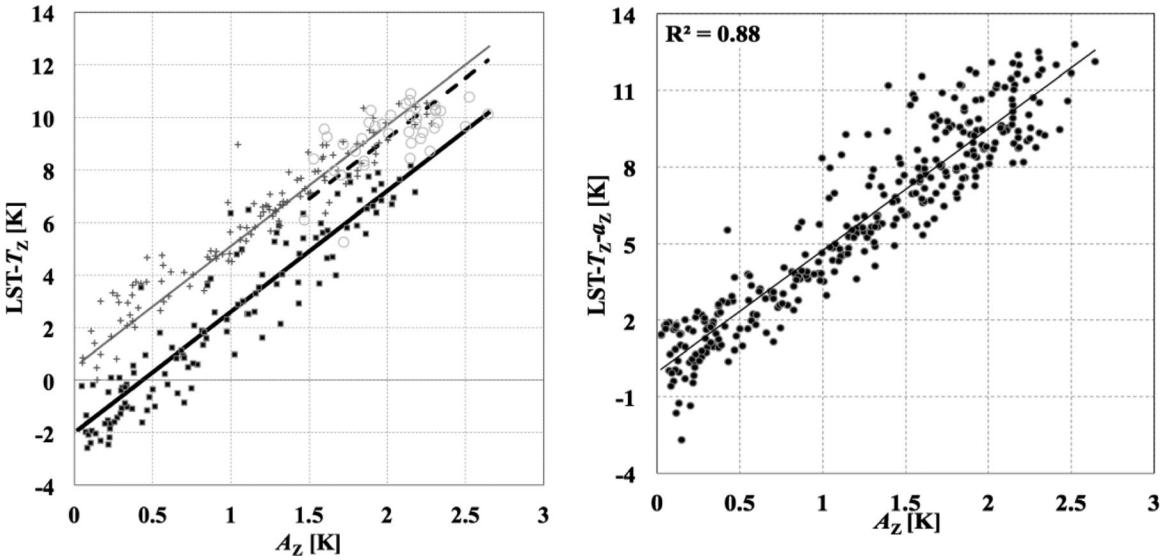

Figure 3. Comparison of A_Z versus (LST − T_Z) at FT_1 for data set *200710*. (left) Samples collected during the morning (black squares), at noon (circles) and afternoon (grey crosses) hours. Black, dashed, and grey lines determined using linear regression analysis. (right) The same samples (left) when the offsets a_{am} and a_{pm} are subtracted to (LST − T_Z); the regression line is forced to the origin.

1982]. By assuming that the offset is fairly constant for a given period during the day, a_{am} and a_{pm} were taken as representative during the morning and afternoon hours. The averaging was done to include the uncertainty that arises when, in practical applications, a is determined. That is, LST may not be always readily available, such as in case of cloudy conditions during sunrise or sunset, or when the spatial coverage of satellites providing images does not match the surface area of interest.

Therefore, for each data set, the samples were split into morning data (collected from sunrise to 11.5 h) and afternoon data (from 12.5 h to sunset). The corresponding offset a_{am} or a_{pm} was used to calculate (LST – T_Z – a) for each sample. All together, the (LST – T_Z – a) samples were compared against A_Z using linear regression analysis forced through the origin. Therefore, the representative s_Z for the data set is the slope of the linear regression analysis. The latter was compared with the parameter s_Z estimated from equation (9).

Overall, the different magnitude of a_{am}, a_{pm}, and parameter s_Z over periods of about 20 days allow checking their robustness through the seasons and the reliability of equation (9) under different conditions. In equation (9) d and z_{0m} were estimated as a portion of the canopy height (see appendix B).

3.4. Sensible Heat Flux Calculation

3.4.1. The SR-LST Method

Starting at neutral conditions, equation (10) and the corresponding wind log-law (see appendix B), were iterated until convergence for u^* was achieved. The iteration stopped when the difference in u^* between two consecutive iterations was less than 0.005 ms^{-1}.

Table 1. Analysis of the Linear Relationship Between A_Z and (LST − T_Z) at FT_1[a]

Data Set	N	ΔTIR (K)	Thermal Status	a_{am} (K)	a_{pm} (K)	s_Z	R^2
140510	651	2	isothermal	−2	1	4.6	0.84
100610	491	3	isothermal	−2	1	4.5	0.89
060710	665	11	anisothermal	−0.5	0.5	4.7	0.84
200710	384	17	anisothermal	−2	0.5	4.6	0.88
030810	404	22	anisothermal	−2	1	4.6	0.83
020910	148	28	anisothermal	−2	1	4.4	0.82
All	2743					4.6	0.87

[a]For each data set it is shown the number of samples available, N, the averaged soil-canopy temperature difference, ΔTIR, the mean offsets at sunrise and at sunset, a_{am} and a_{pm}, respectively, the parameter s_Z and the coefficient of determination, R^2. The data sets were labeled as isothermal surface for $\Delta TIR \leq 3$ K and anisothermal otherwise.

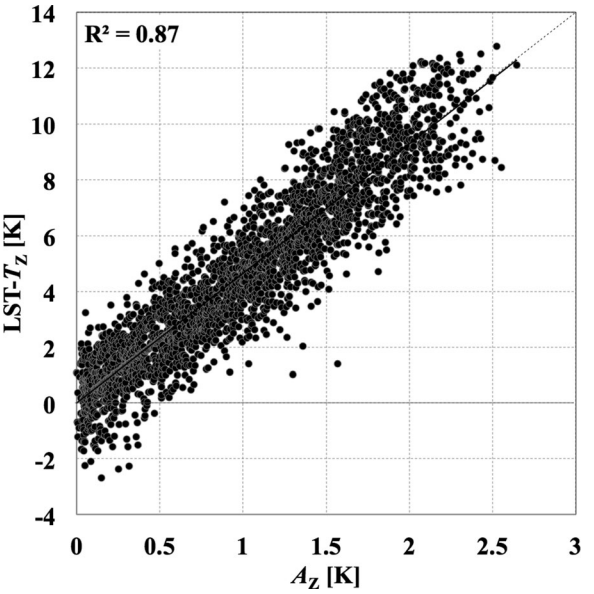

Figure 4. Scatterplot between A_Z and offset-corrected (LST − T_Z) for all the data sets collected at FT_1.

3.4.2. The One-Source Bulk Transfer Formulation

At FT_2, the same procedure was applied to determine the sensible heat flux in the inertial sublayer using the one-source bulk transfer formulation (H_{MOST}) (equations (A3) and (A4)). The parameter kB^{-1} was optimized minimizing the RMSD comparing H_{MOST} against H_{EC}.

4. Results and Discussion

4.1. The Parameters a_{am}, a_{pm}, and s_Z

4.1.1. *Tower* FT_1

The two-step process used to determine s_Z is shown for data set *200710* (Figure 3), and it reveals significant differences between offsets a_{am} and a_{pm} (Figure 3a), as well as that, after removing the corresponding offset for each sample shown in Figure 3a, the general trend observed was indeed linear (Figure 3b). For samples collected at noon the offset was set to zero. The Figures 3a and 3b show that the samples at noon scattered around the general linear trend. The representative parameter s_Z for this data set was determined by forcing the linear regression through the origin for all the data (Figure 3b). The behavior for the remaining data sets was similar.

For each data set, the offsets a_{am} and a_{pm}, parameter s_Z, and the coefficient of determination (R^2) of the linear regression analysis, including the number of samples available (N), the LST gradient (ΔTIR), and the corresponding thermal status of the surface are reported in Table 1.

For a given period, a_{am} and a_{pm} are different (Table 1); they have different signs in all the cases and they vary in time. However, the parameter s_Z remains fairly constant. A surface like an olive orchard can be split in two displaced sources of heat fluxes (i.e., the soil and the canopy), and their different strengths seemed not to play a role in either parameter s_Z or in the magnitude of the mean offsets. The coefficient R^2 was high, in the range of $0.82 \leq R^2 \leq 0.89$ and the coefficient of variation (CV) of the mean s_Z values (Table 1) was small, CV = 0.02.

The comparison of A_Z versus the offset-corrected (LST − T_Z) (Figure 3b) for all the data (Figure 4) shows that the slope of the linear regression analysis forced through the origin was $s_Z = 4.6$, and the correlation was high, $R^2 = 0.87$. Therefore, a single parameter s_Z holds for the entire campaign. Given that the canopy height was fairly constant along the campaign and that s_Z seems independent of the strength and vertical distribution of the sources of heat, a constant s_Z agrees with the modeling approach described in equation (9). Therefore, equation (9) was reliable, regardless of the heterogeneity and the thermal status of the surface.

Table 2. Validation of the Sensible Heat Flux at FT_1[a]

	Versus EC					Versus BREB				
Data Set	*N*	*m*	*q*	R^2	RMSD	*N*	*m*	*q*	R^2	RMSD
140510	609	1.10	−1*	0.78	73, 39%	606	0.92	−11	0.84	65, 29%
100610	442	1.07	−8	0.78	74, 38%	290	0.98	−20	0.79	62, 28%
060710	611	1.20	−6	0.90	42, 20%	503	0.82	−3*	0.86	61, 25%
200710	351	1.01	−1*	0.88	50, 21%	269	0.84	18	0.83	69, 26%
030810	372	1.02	20	0.80	67, 29%	316	0.72	18	0.65	84, 32%
020910	140	1.21	−7*	0.87	74, 32%	135	1.10	−6	0.82	57, 25%
All	2525	1.05	−8	0.78	59, 27%	2119	0.89	−3*	0.81	65, 27%

[a]Method SR-LST versus methods EC and BREB. For each data set and for all the data it is shown *N*, *m*, *q* (W m^{-2}), and R^2 of the linear regression analysis and the RMSD (W m^{-2}) is also expressed over the mean *H* taken as a reference (%). Subscript asterisk (*) indicates that coefficient *q* is statistically negligible (5% level of significance).

Table 3. Validation of the Sensible Heat Flux at FT_2[a]

	Versus EC					Versus BREB				
Data Set	*N*	*m*	*q*	R^2	RMSD	*N*	*m*	*q*	R^2	RMSD
140510	642	1.10	−6	0.91	44, 24%	609	0.97	9	0.90	50, 23%
100610	289	1.06	−13	0.79	60, 30%	209	0.92	−15	0.83	62, 28%
060710	571	1.12	−16	0.88	45, 22%	530	0.90	−18	0.77	50, 22%
200710	12	1.00	3	0.90	43, 18%	12	0.85	−4	0.94	40, 15%
030810	250	1.10	−37	0.88	52, 23%	236	0.90	−12	0.75	80, 30%
020910	123	1.04	0	0.87	48, 22%	123	1.00	−24	0.85	59, 26%
All	1887	1.08	−15	0.88	49, 22%	1719	0.96	1	0.85	56, 23%

[a]Method SR-LST versus methods EC and BREB. For each data set and for all the data it is shown *N*, *m*, *q* (W m^{-2}), and R^2, of the linear regression analysis and the RMSD (W m^{-2}) is also expressed over the mean *H* taken as a reference (%). (*) Coefficient *q* is statistically negligible (5% level of significance).

4.1.2. *Tower* FT_2

Because raw high-frequency data of air temperature were not available, the ramp amplitude and, therefore, the parameter s_Z could not be determined. The offset pairs (a_{am}, a_{pm}) determined for each data set were (−2, −1), (−2.5, −2), (−1.5, −1), (−2.25, −1.25), (−3, −1.5), and (−2, −1) for data sets *140510*, *100610*, *060710*, *200710*, *030810*, and *020910*, respectively. In contrast to tower FT_1 where a_{pm} was consistently positive, at FT_2 it was consistently negative. Because the role of the offset is to correct for the difference between LST and aerodynamic temperature, it is difficult to explain the variability of the offset because the aerodynamic temperature cannot be directly measured. Because at FT_2, the LST was estimated and the irrigation scheduling was different, it was difficult to discern the reasons for such different magnitudes.

4.1.3. Estimating the Parameter s_Z

Because the height of the roughness sublayer is about two times the canopy height (i.e., the roughness sublayer varies with stability conditions) [*Brutsaert*, 1982; *Mölder et al*., 1999], instrumentation at towers FT_1 and FT_2 mainly remained within the roughness and inertial sublayer, respectively. The parameters s_Z estimated according to equation (9) were $s_Z = 4.53$ and $s_Z = 7.0$ at FT_1 and FT_2, respectively; the value obtained for FT_1 is in close agreement with the slope value obtained for the whole data set, as reported in Table 1 and Figure 4. The exact same value observed for all the data, $s_Z = 4.6$ (Table 1), is obtained for $h = 3.26$ m in equation (9). The reliability of the parameter s_Z at FT_2 could only be tested indirectly (i.e., through validation of the sensible heat flux).

4.2. Validation of the $H_{SR\text{-}LST}$ Estimates

At FT_1 and FT_2 (Tables 2 and 3, respectively), $H_{SR\text{-}LST}$ was compared against the two references (EC and BREB methods). For each data set, *N*, slope (*m*), intercept (*q*), and R^2 of the linear regression analysis were determined, as well as the RMSD.

4.2.1. *Tower* FT_1

The R^2 coefficient values against the EC method were in the range of $0.78 \leq R^2 \leq 0.90$, with the highest correlations observed when the surface behaved as anisothermal. The correlations against the BREB method were similar overall. The intercept values were small, even if they were statistically negligible only for two data sets (at 5% level of significance). Regardless of the reference, the RMSD values were in the range of 42 W $m^{-2} \leq$ RMSD $\leq$ 84 W m^{-2}; thus, in general, similar to the RMSD obtained by comparing the two reference data sets to each other for all the data (RMSD = 62 W m^{-2}). The relative RMSD values (ratio between RMSD and the mean *H* ($\overline{H}$)), were in the range of $20\% \leq \text{RMSD}/\overline{H}_{EC} \leq 39\%$ and $25\% \leq \text{RMSD}/\overline{H}_{BREB} \leq 32\%$; therefore, comparable with the usual accuracy of the two methods taken as a reference [*Allen et al*., 2011]. Thus, in general, when the instrumentation was deployed in the roughness sublayer, equation (10) performed reliably throughout the campaign.

4.2.2. *Tower* FT_2

Compared to FT_1, the RMSD and RMSD/$\overline{H}$ values were smaller and the slopes were closer to one (Table 3). For all data, RMSD = 49 W m^{-2} and 56 W m^{-2} with a relative error of 22% and 23%, and; $m = 1.08$ and 0.96 against methods EC and BREB, respectively. Also for this olive grove, RMSD values were close to the RMSD obtained by inter-comparing the two references for all data (RMSD = 53 W m^{-2}). Regardless of the reference, the coefficients R^2 were in the range of $0.75 \leq R^2 \leq 0.91$. Therefore, equation (10) also performed reliably in the inertial sublayer. Partly, the better performance of equation (10) observed when operating in the inertial sublayer than in the roughness sublayer may be as a consequence that for the former the roughness

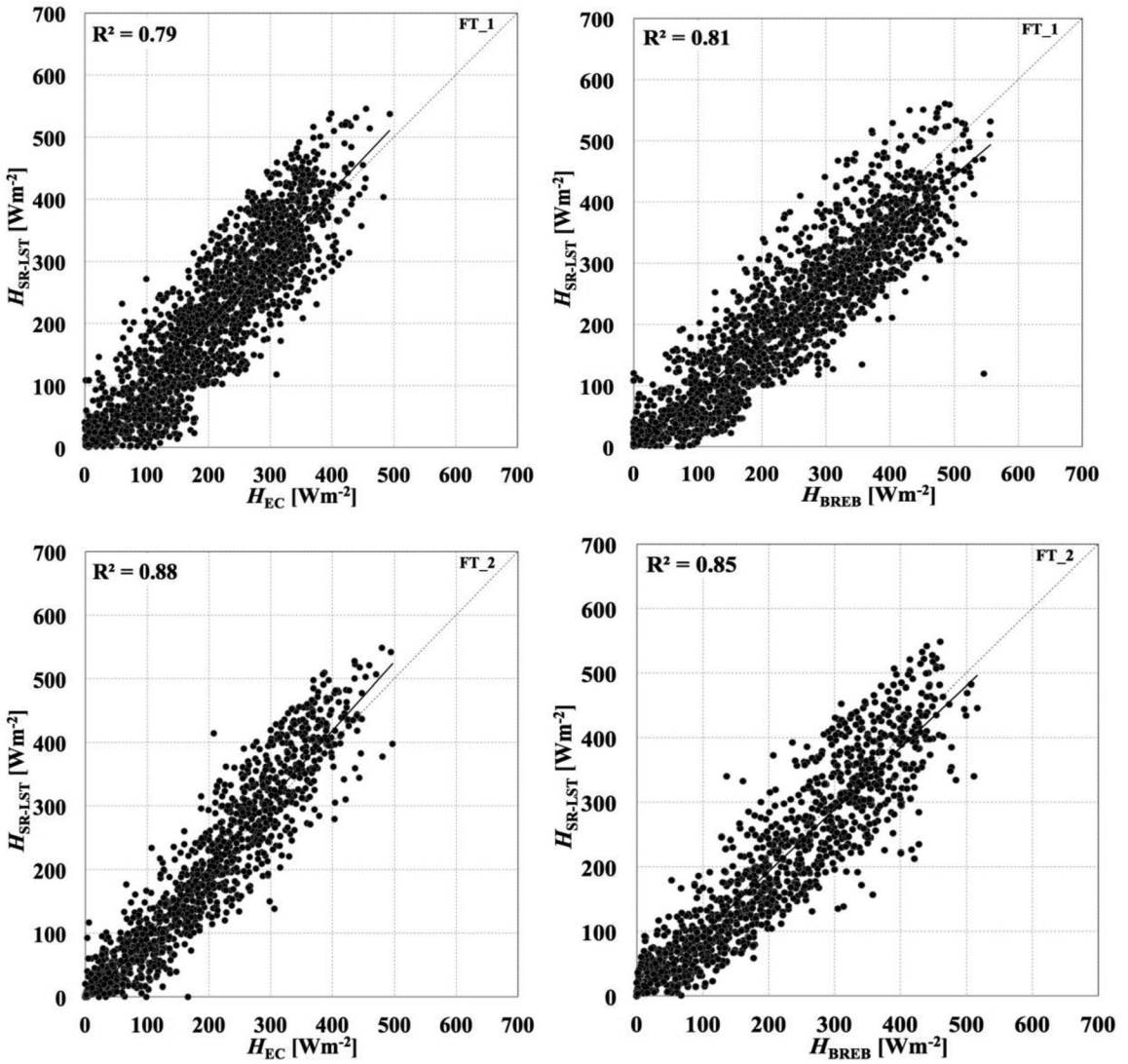

Figure 5. Scatterplot of the sensible heat flux determined using the method SR-LST versus the (left) EC method and (right) BREB method at (top) towers FT_1 and (bottom) FT_2.

sublayer depth is not required as input. To minimize input requirements, and as a consequence of the assumption that high frequency measurements are not available, the roughness sublayer was assumed to remain constant though it varies with stability conditions [*Graefe*, 2004; *Castellví et al*., 2012].

A comparison between the sensible heat flux determined using the SR-LST method versus the EC and BREB observations for all the data (Figure 5) shows that regardless of the olive grove and the reference used for comparison, for a few samples the SR-LST method tended to overestimate the highest fluxes, which suggests that around noon under clear skies (free convection) equation (10) may require some refinement. However, it is well known that the EC method tends to underestimate the actual heat flux under free convection [*Sakai et al*., 2001], and it is not clear if the BREB method can provide reliable partition of the actual sensible and latent heat fluxes [*Cuxart et al*., 2015]. Because the offset was set to zero for samples collected at noon, some refinement on equation (10) may be implemented by simply subtracting a positive offset to (LST $- T_Z$). However, performing other experiments could elucidate how to address this issue.

4.3. Validation of the H_{MOST} Estimates

In order to have a benchmark comparison of the performance of the SR-LST method, H_{MOST} (see equation (A3)) was determined at site FT_2 because instrumentation operated in the inertial sublayer. The first choice for parameter kB^{-1} was the recommended value for homogeneous canopies ($kB^{-1} = 2$). But the latter

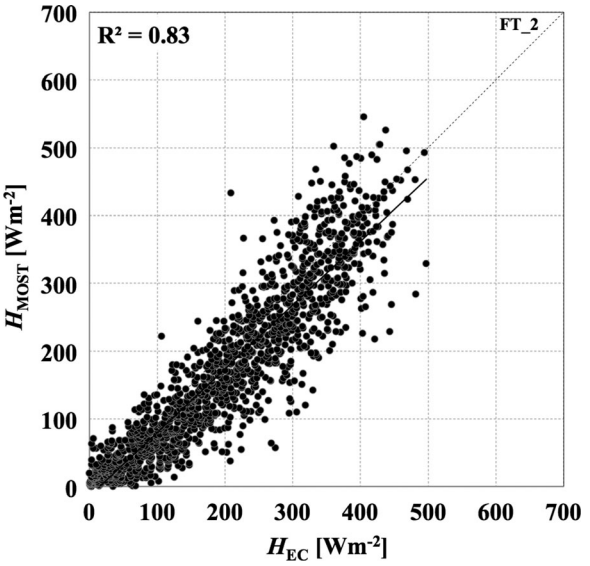

Figure 6. Scatterplot of the sensible heat flux determined using the calibrated one source bulk transfer formulation (H_{MOST}) versus the EC method for all data at FT_2.

overestimated the reference H_{EC} by a factor of two. Because at FT_2 the offsets a_{am} and a_{pm} were negative, their implementation to correct $(LST-T_Z)$ during the morning and afternoon hours would enhance the overestimation of H_{MOST} in relation to H_{EC}. Therefore, $(LST-T_Z)$ was not corrected and the parameter kB^{-1} was calibrated. The first data set, *140510*, was used to determine the kB^{-1} value that minimized the RMSD. The optimized kB^{-1} was $kB^{-1} = 6.01$ which was taken as representative for the other data sets. A method based on Simulating Annealing (SA) was used to solve for kB^{-1} [*Goffe et al*., 1994]. SA is a global optimization method that distinguishes between different local optima. By giving boundaries for kB^{-1}, starting from an initial kB^{-1}, the algorithm takes a random step and the RMSD is evaluated. Decisions of minimums and maximums of the target function (RMSD) is made by a Metropolis criteria [*Metropolis et al*., 1953] which can even take steps falling out of the boundaries. As the optimization process proceeds, the length of the steps decline until it closes in a global optimum. To minimize the target function RMSD, the range of variability assigned to kB^{-1} was wide, $1 \leq kB^{-1} \leq 9$.

The data in Table 4 show the results of the linear regression analysis and the RMSD values obtained by comparing H_{MOST} versus H_{EC} for each data set and for all data. The scatterplot in Figure 6 shows the comparison H_{MOST} versus H_{EC} for all data. H_{MOST} was close to H_{EC} and, in comparison to the SR-LST method (Figure 5, left), the Figure 6 shows that H_{MOST} tended to perform slightly closer than $H_{SR\text{-}LST}$ for the highest values of H_{EC}. However, considering all the range of stabilities, the Table 4 shows that the RMSD obtained using the method SR-LST was in general smaller than the obtained using MOST. Optimization of parameter kB^{-1} for each data set was within the range $4.75 \leq kB^{-1} \leq 6.15$, and the RMSD values obtained were similar than those shown in Table 4 (i.e., the differences never exceeded 6 W m^{-2}). Thus, in practice MOST (after the site-specific calibration) and SR-LST performed similar.

5. Summary and Concluding Remarks

An SR-based equation for estimating H has been proposed which involves LST as input without requiring the ramp duration (equation (6)). On this basis, an approach to estimate H was proposed for moderately sparse vegetation and tested over an olive orchard (equation (10)). The proposed approach assumes a linear relationship between A_Z and $(LST - T_Z)$ (equation (5)), exploiting the concept that equation (5) can be parameterized using the canopy height and measurements of LST at neutral conditions (i.e., sunset or sunrise) as input. The crucial assumption that the slope in equation (5) remains fairly constant during daytime hours

Table 4. Validation at FT_2 of the Sensible Heat Flux Using the One Source Bulk Transfer Formulation Using the Parameter kB^{-1} Calibrated for Data Set 140510[a]

	Versus EC				
Data Set	*N*	*m*	*Q*	R^2	RMSD
140510	642	1.00	−7	0.87	49, 27%
100610	289	0.94	−28	0.77	70, 30%
060710	571	0.98	−19	0.86	54, 22%
200710	12	0.71	17	0.83	74, 18%
030810	250	0.90	−23	0.85	66, 23%
020910	123	1.03	−27	0.89	48, 22%
All	1887	0.94	−14	0.83	58, 22%

[a]For each data set and for all the data it is shown *N*, *m*, *q* (W m^{-2}), and R^2, of the linear regression analysis and the RMSD (W m^{-2}) is also expressed over the mean *H* taken as a reference the EC method (%) which was used for calibration.

was checked and the results obtained confirm that such hypothesis is reliable. Estimation of offset in equation (5) requires multitemporal LST acquisitions because at sunrise and sunset varied without following a clear pattern. Regardless of season or measurement height, H estimates were generally comparable to those determined using the EC or BREB methods. Under free convection, H may overestimate these two references. Further observations are required to confirm this as a general issue.

The method proposed for estimating H seems a valuable alternative to bulk transfer formulations; in particular, the SR-LST method requires the same inputs of the one-source model at the estimation time (LST, T_Z, u_Z, and h), and the additional information required at neutral conditions (LST at sunrise/sunset) alleviate the problem related to the discrepancy between aerodynamic temperature and LST. In addition, if LST is measured with the same instrument, the offset may correct for a possible inconsistency between air temperature and LST in its retrieval. The latter two uncertainties are the main drawbacks of the one-source formulations. A clear outcome of the study is that an operational application of the proposed methodology on satellite images requires a pair of LST data, the first acquired under the condition $H = 0$ (sunset/sunrise) and the second during daytime. As a consequence, the method is suitable for applications based on data collected by geostationary satellites (e.g., the Meteosat Second Generation (MSG) and the Geostationary Operational Environmental Satellite [GOES]), which are usually characterized by a high temporal resolution (≈15 min). Additionally, *Guzinski et al.* [2013] demonstrated that night-time acquisitions of the Moderate Resolution Imaging Spectroradiometer (MODIS) can be successfully used as proxy of sunrise observations for land-surface modeling. As an extension, all the satellites with a pair of night/day thermal acquisitions (e.g., Landsat where available) are potentially suitable for the application of the proposed method. Additionally, since the model semiempirical parameters (a and s_z) are locally calibrated, the extension of the methodology to satellite images only requires a pixel-by-pixel application of the proposed calibration methodology. In this case pixel-by-pixel meteorological values may be retrieved through classical geo-statistical methods.

Fetch requirements for SR-flux approaches and EC method are identical [*Castellví*, 2012], which may be considered to estimate the measurement height to match as much as possible the spatial coverage of the image. The one-source bulk transfer formulation operating in the inertial sublayer for estimating H required calibration of parameter kB^{-1}. After calibration, the latter performed similar to SR-LST method.

It is concluded that A_Z and (LST $- T_Z$) are linearly related over heterogeneous canopies and that this relationship can be parameterized using affordable input over wide periods were near-neural and unstable conditions are met (i.e., typically during daytime); consequently, the SR method proposed seems a viable alternative to estimate the sensible heat flux for remote sensing applications.

Appendix A: Estimation of Coefficient λ_h, the Roughness Sublayer Depth, the One-Source Bulk Transfer Formulation for Estimating H and Estimation of Parameters s_Z and a at Near-Neutral Conditions

A1. Coefficient λ_h

Because the friction velocity (u_*) and the ramp period (τ) remain fairly constant above the canopy [*Paw et al.*, 2005], it allows proposing the following relationship for coefficient λ_h in equation (3):

$$\frac{1}{\tau u_*} = \frac{\lambda_h}{h} = \frac{\lambda_Z}{Z}, \tag{A1}$$

where h is the canopy height and λ_Z is a coefficient that suits at height Z above the ground. The coefficient λ_Z was determined for different surfaces [*Chen et al.*, 1997b]; $\lambda_Z = 0.4$ was obtained under convective conditions for bare soil at $Z = 0.03$ m; $\lambda_Z = 0.54$ was obtained under unstable cases for straw mulch (0.06 m thick) at $Z = 0.09$ m, and; $\lambda_Z = 0.7$ was obtained under near neutral and unstable conditions for fir-forest (16.7 m tall) at $Z = 23$ m. Thus, excluding bare soils and mulches, as a rule of thumb, an averaged coefficient λ_h may suit for a moderately heterogeneous canopy under near neutral and unstable conditions because such a surface may combine portions of bare soil and short understories below the ove11rstory. Thus, $\lambda_h = 0.55$.

A2. The Roughness Sublayer Depth Above the Zero-Plane Displacement

Under near neutral conditions, the height z^* can be estimated as [*Castellví and Snyder*, 2010]; $z^* = 4.71h\alpha^2_{z=h}$, where $\alpha_{Z=h}$ is the parameter α_Z determined at the canopy top that corrects for the uneven heating in the

earlier SR-flux equation (equation (1)). Excluding bare soils and highly heterogeneous canopies, such as savannah, field studies and wind tunnel experiments have shown that $\alpha_{Z=h}$ is in the range of $0.5 \leq \alpha_{Z=h} \leq 0.6$ under neutral conditions [*Paw et al*., 1995; *Katul et al*., 1996; *Castellví and Snyder*, 2010]. Thus, $\alpha_{Z=h} = 0.55$ can be taken as a intermediate value and the following approach to estimate z^* at neutral conditions is proposed:

$$z^* = 1.4h \tag{A2}$$

A3. The One-Source Bulk Transfer Formulation for Estimating H

The one-source bulk transfer formulation based on Monin - Obukhov Similarity Theory (MOST) estimates the sensible heat flux (H_{MOST}) by integrating the flux-gradient relationship from the roughness length for heat transfer (z_{0h}) up to a given height of reference above the zero-plane displacement (z). Typically, H_{MOST} is expressed as [*Brutsaert*, 1982]:

$$H_{MOST} = \rho C_p \frac{(T_0 - T)}{r_{ah}}, \tag{A3}$$

where T is the air temperature measured at z, T_0 is the aerodynamic air temperature defined as the extrapolated temperature of the air at the roughness length for heat transfer (z_{0h}) following the profile predicted by MOST, and r_{ah} is the aerodynamic resistance:

$$r_{ah} = \frac{1}{k u_*}\left(\ln\left(\frac{z}{z_{0m}}\right) + kB^{-1} - \Psi_{h(z/L)} + \Psi_{h(zoh/L)}\right), \tag{A4}$$

where kB^{-1} is a parameter defined as, $kB^{-1} = \ln\left(\frac{z_{0m}}{z_{0h}}\right)$ being z_{0m} the roughness length for momentum, and $\Psi_{h(z/L)} = 2\ln\left(\frac{1+y^2}{2}\right)$ where y is the momentum exchange universal function: $y = \left(1 - 16\frac{z}{L}\right)^{0.25}$ [*Dyer*, 1974].

A4. Parameters s_Z and a

The earlier SR-flux equation estimates the sensible heat flux (H_{SR1}) as *Paw et al*. [1995]:

$$H_{SR1} = \rho\, C_p \frac{(\alpha_z Z)}{\tau} A_Z. \tag{A5}$$

Because MOST is restricted to the inertial sublayer, combining (A3) and (A5) allows writing the following relationship valid in the inertial sublayer:

$$(T_0 - T_Z) = s_Z A_Z, \tag{A6}$$

where $s_Z = r_{ah}\frac{(\alpha_Z Z)}{\tau}$ expresses a ratio between the vertical velocity scale for the transfer of a scalar (W_s) predicted by MOST, $W_s = \frac{1}{r_{ah}}$, and the predicted by SR analysis, $W_s = \frac{\alpha_Z Z}{\tau}$. Because z0h is a height within the canopy, the aerodynamic temperature is presumed to be related with LST [*Brutsaert*, 1982; *Crago and Qualls*, 2014], and from (A6) the following relationship is proposed:

$$(LST - T_Z) = s_Z A_Z + a, \tag{A7}$$

where a is an offset that accounts for the discrepancy between the aerodynamic temperature and the land surface temperature, $a = (\mathrm{LST} - T_0)$. For applications in remote sensing it has been assumed that the aerodynamic temperature equals the land surface temperature which allowed estimating the sensible heat flux from (A3) involving LST as input. The latter predicts that $(\mathrm{LST} - T_Z)$ is zero at neutral conditions. However, observations often show that $(\mathrm{LST} - T_Z)$ cannot be neglected at neutral conditions, especially over sparse anisothermal canopies [*Boulet et al*., 2012].

A5. Determining Parameters a and s_Z at Neutral Conditions

Provided that LST is available, from (A7) the offset a can be determined at neutral conditions, such as around sunrise and sunset as:

$$a_{(z/L=0)} = LST_{(z/L=0)} - T_{Z(z/L=0)}. \tag{A8}$$

Under near neutral conditions, regardless of the measurement height above the canopy, the parameter α_Z is close to $\alpha_Z = 0.5$ [*Castellví*, 2004]. The aerodynamic resistance determined at neutral conditions is $r_{ah(z/L=0)} = \frac{1}{k u_*}\left(\ln\left(\frac{z}{z_{0m}}\right) + kB^{-1}\right)$, and over sparse canopies *Kustas et al*. [1989] observed

that when $(\mathrm{LST}-T_Z)$ tends to zero, the parameter kB^{-1} is close to 2 (i.e., 2.2), which is the value recommended over homogeneous canopies regardless of the stability case. Therefore, for homogenous and moderately heterogeneous canopies under near-neutral conditions it is proposed to estimate $s_Z = r_{ah}\frac{(\alpha_Z Z)}{\tau}$ as:

$$s_Z = \left(\frac{\lambda_h}{2k}\frac{Z}{h}\right)\left(\ln\left(\frac{z}{z_{0m}}\right)+2\right) \text{ with } \lambda_h = 0.55. \tag{A9}$$

Here, it is assumed that under neutral conditions the log-profiles of the wind speed and air temperature predicted by MOST are still reliable in the upper part of the roughness sublayer [*Harman and Finnigan*, 2007, 2008; *Arnqvist and Bergström*, 2014]. The latter allows applying (A9) when the measurement height is not too close to the canopy top. For bare soils, likely, determination of coefficient λ_z at a typical measurement height for a wide range of stability conditions is convenient for estimating s_z as:

$$s_Z = \left(\frac{\lambda_z}{2k}\right)\left(\ln\left(\frac{Z}{z_{0m}}\right)+2\right). \tag{A10}$$

Appendix B: Determination of Friction Velocity and Roughness Parameters

After defining the relative height of the roughness sublayer, the friction velocity can be estimated within the inertial sublayer or within the roughness sublayer using appropriate equations.

When the horizontal mean wind speed, u_Z, is measured within the inertial sublayer, the friction velocity can be estimated using the wind log-law [*Brutsaert*, 1982]:

$$u_* = \frac{k u_Z}{\ln\left(\frac{z}{z_{0m}}\right) - \Psi_{m(z/L)} + \Psi_{m(z_{0m}/L)}} \text{ with } Z \geq Z^*, \tag{B1}$$

where L is the Obukhov length; $\Psi_{\mathrm{m}\ (z/L)}$ and $\Psi_{\mathrm{m}\ (z0m/L)}$ are the integrated stability function for momentum transfer measured at z/L and at z_{0m}/L, respectively; z^* is the height (above d) of the roughness sublayer, Z^*. The integrated stability correction functions for momentum is:

$$\Psi_{m(z/L)} = \int_0^z \left[1-\varphi_{h(x)}\right]\frac{dx}{x} = 2\ln\left(\frac{1+y}{2}\right)+\ln\left(\frac{1+y^2}{2}\right)-2\arctan y+\frac{\pi}{2}. \tag{B2}$$

When the wind speed is measured in the roughness sublayer, the friction velocity may be expressed as [*Cellier and Brunet*, 1992]:

$$u_* = \frac{u_Z}{\lambda_2 + \frac{1}{k}\left(\left(\frac{z-h+d}{z^*}\right) - \Psi^*_{m(z/L)} + \Psi^*_{m((h-d)/L)}\right)} \text{ with } h \leq \ Z \leq Z^*, \tag{B3}$$

where h is the canopy height, λ_2 is the ratio between the friction velocity and the wind speed measured at the canopy top [*Graefe*, 2004], and $\Psi^*_{m(z/L)}$ denotes the appropriate $\Psi_{m(z/L)}$ within the roughness sublayer. For low-density canopies:

$$\Psi^*_{m(z/L)} = \frac{z}{z^*}\frac{\left(y^4-\frac{4}{3}y^3+\frac{1}{3}\right)}{\left(y^4-1\right)}. \tag{B4}$$

At neutral conditions, by equating (B1) and (B4) at $z = z^*$ the following relationship is obtained for $\lambda_2 = \frac{u_h}{u_*}$,

$$\lambda_2 = \frac{1}{k}\left(\ln\left(\frac{z^*}{h}\right)+\ln\left(\frac{h}{z_{0m}}\right)-1+\left(\frac{h-d}{z^*}\right)\right). \tag{B5}$$

Therefore, in agreement with (A2) which assumed $\alpha_{Z=h} = 0.55$, $\frac{z^*}{h} = 1.425$, and using as a benchmark typical ratios for $\frac{d}{h}$ and $\frac{z_{0m}}{h}$, such as $\frac{d}{h} = 0.7$ and $\frac{z_{0m}}{h} = 0.125$ [*Graefe*, 2004; *Raupach*, 1994; *Brutsaert*, 1982], the coefficient λ_2 at neutral conditions is $\lambda_2 = 4.0$, and it was assumed to perform constant.

Notation

α_z	Parameter that corrects for the uneven heating of the air parcel. Semiempirical parameter in H_{SR_1}.
$\alpha_{Z=h}$	α_Z determined at the canopy top.
δ	Semiempirical parameter of the H_{SR} approach.
ε_0	Surface emissivity.
ε_v and ε_s	Canopy and soil emissivity, respectively.
γ	Enhancement correction factor of $\varphi_{h(z/L)}^{-1}$.
λ_1	Ratio between the wind shear at the canopy and the ramp period.
λ_2	Ratio between the friction velocity and the wind speed at the canopy top.
λ_h	Product between λ_1 and λ_2.
λ_Z	Coefficient in equation (A1) that suits at height Z.
λET	Latent heat flux, W m^{-2}.
$\phi_{h(z/L)}$	Stability function for heat transfer.
ρ	Air density, kg m^{-3}.
σ	Stefan-Boltzmann constant, W m^{-2} K^{-4}.
τ	Ramp period determined using measurements taken at high frequency, s.
ΔTIR	Absolute difference between the average values *TIRs* and *TIRc*, K.
Ψ_h and Ψ_m	Integrated stability function for heat transfer and momentum, respectively, in the inertial sublayer. With subscript * valid in the roughness sublayer.
m and q	Slope and intercept of $H_{SR\text{-}LST}$ versus the measured H, W m^{-2}.
a	Difference between the land surface temperature and the air temperature measured at Z at neutral conditions. Also intercept of the linear relationship in equation (5), K.
a_{am} and a_{pm}	a at sunrise and sunset, respectively. K.
d	Zero-plane displacement, m.
f_s	Fraction of exposed soil.
h	Canopy height, m.
k	von-Kármán constant
$_{kB}^{-1}$	Natural logarithm of the ratio between momentum and heat roughness lengths
s_Z	Ratio between the vertical surface velocity scale for heat transfer predicted by MOST and SR analysis. Also slope of the linear relationship in equation (5),
u_h	Horizontal mean wind speed at the canopy top, ms^{-1}.
u_*	Friction velocity, ms^{-1}.
x	Integration variable z/L.
y	Momentum exchange universal function for momentum.
z	Measurement height above d, m.
z^*	Height of the roughness sublayer above d, m.
z_{0h}	Roughness length for heat transfer, m.
z_{0m}	Roughness length for momentum, m.
A_Z	Ramp amplitude observed at Z determined using measurements taken at high frequency, K.
C_p	Isobaric specific heat capacity, J kg^{-1} K^{-1}.
ET	Evapotranspiration, mm.
G	Soil heat flux, W m^{-2}.
H	Sensible heat flux, W m^{-2}.
H_{BREB}	H determined using the BREB method, W m^{-2}.
H_{EC}	H determined using the EC method, W m^{-2}.
H_{SR}	H determined using SR, W m^{-2}.
H_{SR_1}	H determined using the original SR equation, W m^{-2}.
$H_{SR\text{-}LST}$	H determined using the proposed method, W m^{-2}.
L	Obukhov length, m.
LST	Land Surface Temperature, K.
R^2	Coefficient of determination.
R_{lu} and R_{ld}	Upwelling and downwelling long-wave radiation, respectively, W m^{-2}.

R_n	Net Radiation, W m^{-2}.
S	Unit surface, m^2.
TIR_s and TIR_c	Half-hourly radiometric temperatures of the soil and canopy, respectively, K.
T_b	Temperature of the air parcel in the streamwise above the canopy, K.
T_0	Aerodynamic temperature, K.
T_Z	Mean air temperature at reference height, K.
V	Volume of the air parcel, m^3.
Z	Measurement height above the ground, m.
Z^*	Roughness sublayer depth above the ground, m.

Acronyms

ALEXI	Atmosphere-Land Exchange Inverse model
BR	Bowen ratio
BREB	Bowen Ratio Energy Balance method
CV	Coefficient of variation
DTD	Dual-Temperature-Difference method
EC	Eddy Correlation method
GOES	Geostationary Operational Environmental Satellite
MOST	Monin - Obukhov Similarity Theory
MODIS	Moderate resolution Imaging Spectroradiometer
MSG	Meteosat Second Generation
N	Number of samples
FT_1 and FT_2	Flux towers 1 and 2
TSEB	Two Source Energy Balance model
SA	Simulating annealing
SEB	Surface Energy Balance
SR	Surface Renewal
SR-LST	Surface Renewal involving LST
RMSD	Root mean square difference

Acknowledgments

The authors thank L. Pasotti, N. Drago, G. Dimino and A. Sammartano of SIAS (*Servizio Informativo Agrometeorologico Siciliano*) for their assistance and to Asun, Carla and Tània who provided access to different facilities in Lleida. This research was funded by project CGL2012-37416-C04-01 and CGL2015-65627-C3-1-R (*Ministerio de Ciencia y Innovación of Spain*), CEI Iberus, 2014 (*Proyecto financiado por el Ministerio de Educación en el marco del Programa Campus de Excelencia Internacional of Spain*), and Ayuda para estancias en centros extranjeros (*Ministerio de Educación, Cultura y Deporte of Spain*). To acquire the database used in this manuscript contact co-authors G. Ciraolo and F. Rossi.

References

Allen, R. G., M. Tasumi, A. Morse, and R. Trezza (2005), A Landsat-based energy balance and evapotranspiration model in Western US water rights regulation and planning, *Irrig. Drain. Syst.*, *19*, 251–268.

Allen, R. G., L. S. Pereira, T. A. Howell, and M. E. Jensen (2011), Evapotranspiration information reporting: I. Factors governing measurement accuracy, *Agric. Water Manage.*, *98*, 899–920.

Anderson, F. E., R. L. Snyder, R. L. Miller, and J. Drexler (2003), A micrometeorological investigation of a restored California wetland ecosystem, *Bull. Am. Meteorol. Soc.*, *84*(9), 1170–1172.

Anderson, M. C., J. M. Norman, G. R. Diak, W. P. Kustas, and J. R. Mecikalski (1997), A two-source time-integrated model for estimating surface fluxes using thermal infrared remote sensing, *Remote Sens. Environ.*, *60*, 195–216.

Anderson, M. C., et al. (2011), Mapping daily evapotranspiration at field to continental scales using geostationary and polar orbiting satellite imagery, *Hydrol. Earth Syst. Sci.*, *15*, 223–239.

Antonia, R. A., A. J. Chamber, C. A. Friehe, and W. Van Atta (1979), Temperature ramps in the atmospheric surface layer, *J. Atmos. Sci.*, *36*, 99–108.

Arnqvist, J., and H. Bergström (2014), Flux-profile relation with roughness sublayer correction, *Q. J. R. Meterorol. Soc.*, *141*, 1191–1197.

Aubinet, M., et al. (2000), Estimates of the annual net carbon and water exchange of forests: The EUROFLUX methodology, *Adv. Ecol. Res.*, *30*, 113–175.

Bastiaanssen, W. G. M., M. Menenti, R. A. Feddes, and A. A. M. Holtslag (1998), A remote sensing surface energy balance algorithm for land (SEBAL): 1. Formulation, *J. Hydrol.*, *212-213*, 198–212.

Berk, A., L. S. Bernstein, G. P. Anderson, P. K. Acharya, D. C. Robertson, J. H. Chetwynd, and S. M. Adler-Golden (1998), MODTRAN cloud and multiple scattering upgrade with application to AVIRIS, *Remote Sens. Environ.*, *65*, 367–375.

Berkooz, G., P. Holmes, and J. L. Lumley (1993), The proper orthogonal decomposition in the analysis of turbulent flows, *Annu. Rev. Fluid Mech.*, *25*, 539–575.

Blyth, E. M., and A. J. Dolman (1995), The roughness length for heat of sparse vegetation, *J. Appl. Meteorol.*, *34*, 583–585.

Boulet, G., A. Olioso, E. Ceschia, O. Marloie, B. Coudert, V. Rivalland, J. Chirouze, and G. Chehbouni (2012), An empirical expression to relate aerodynamic and surface temperatures for use within single-source energy balance models, *Agric. For. Meteorol.*, *161*, 148–155.

Brutsaert, W. (1982), *Evaporation into the Atmosphere. Environmental Fluid Mechanics*, 299 pp., Kluwer Acad., Dordrecht, Netherlands.

Cammalleri, C. (2011), Modelling water and energy balance of the land-atmosphere system using high resolution remote sensing data, PhD thesis, 307 pp., Univ. of Palermo, Palermo, Italy.

Castellví, F. (2004), Combining surface renewal analysis and similarity theory: A new approach for estimating sensible heat flux, *Water Resour. Res.*, *40*, W05201, doi:10.1029/2003WR002677.

Castellví, F. (2012), Fetch requirements using surface renewal analysis for estimating scalar surface fluxes from measurements in the inertial sub-layer, *Agric. For. Meteorol.*, *152*, 233–239.
Castellví, F. (2013), A method for estimating the sensible heat flux in the inertial sub-layer from high-frequency air temperature and averaged gradient measurements, *Agric. For. Meteorol.*, *180*, 68–75.
Castellví, F., and R. L. Snyder (2009), Combining the dissipation method and surface renewal analysis to estimate scalar fluxes from the time traces over rangeland grass near Ione (California), *Hydrol. Processes*, *23*(6), 842–857.
Castellví, F., and R. L. Snyder (2010), A new procedure based on Surface Renewal analysis for estimating the sensible heat flux. A case study over grapevines, *J. Hydrometeorol.*, *11*, 496–508.
Castellví, F., P. J. Perez, and M. Ibañez (2002), A method based on high frequency temperature measurements to estimate sensible heat flux avoiding the height dependence, *Water Resour. Res.*, *38*(6), 1084, doi:10.1029/2001WR000486.
Castellví, F., R. L. Snyder, and D. D. Baldocchi (2008), Surface energy-balance closure over rangeland grass using the eddy covariance method and surface renewal analysis, *Agric. For. Meteorol.*, *148*, 1147–1160.
Castellví, F., S. Consoli, and R. Papa (2012), Sensible heat flux estimates using two different methods based on surface renewal analysis. A study case over an orange orchard in Sicily, *Agric. For. Meteorol.*, *152*, 58–64.
Castellví, F., P. Gavilan, and M. P. Gonzalez-Dugo (2014), Combining the bulk transfer formulation and surface renewal analysis for estimating the sensible heat flux without involving the parameter kB^{-1}, *Water Resour. Res.*, *50*, 8179–8190, doi:10.1002/2013WR014950.
Cellier, P., and Y. Brunet (1992), Flux-gradient relationships above tall plant canopies, *Agric. For. Meteorol.*, *58*, 93–117.
Chehbouni, A., D. Lo Seen, E. G. Njoku, and B. Monteny (1996), Examination of the difference between radiometric and aerodynamic surface temperatures over sparsely vegetated surfaces, *Remote Sens. Environ.*, *58*, 177–186.
Chen, W., M. D. Novak, T. A. Black, and X. Lee (1997a), Coherent eddies and temperature structure functions for three contrasting surfaces. Part I. Ramp model with finite micro-front time, *Boundary Layer Meteorol.*, *84*, 99–123.
Chen, W., M. D. Novak, T. A. Black, and X. Lee (1997b), Coherent eddies and temperature structure functions for three contrasting surfaces. Part II: Renewal model for sensible heat flux, *Boundary Layer Meteorol.*, *84*, 125–147.
Crago, R. D., and R. J. Qualls (2014), Use of land surface temperature to estimate surface energy fluxes: Contributions of Wilfried Brutsaert and collaborators, *Water Resour. Res.*, *50*, 3396–3408, doi:10.1002/2013WR015223.
Cuxart, J., L. Conangla, and M. A. Jiménez (2015), Evaluation of the surface energy budget equation with experimental data and the ECMWF model in the Ebro Valley, *J. Geophys. Res. Atmos.*, *120*, 1008–1022, doi:10.1002/2014JD022296.
Dash, P., F.-M. Göttsche, F.-S. Olesen, and H. Fisher (2002), Land surface temperature and emissivity estimation from passive sensor data: Theory and practice-current trends, *Int. J. Remote Sens.*, *23*(13), 2563–2594.
Drexler, J. Z., F. E. Anderson, and R. L. Snyder (2008), Evapotranspiration rates and crop coefficients for a restored marsh in the Sacramento–San Joaquin Delta, California, USA, *Hydrol. Processes*, *22*, 725–735.
Dyer, A. J. (1974), A review of flux-profile relationships, *Boundary Layer Meteorol.*, *7*, 363–372.
Finnigan, J. J., R. H. Shaw, and E. G. Patton (2009), Turbulence structure above a vegetation canopy, *J. Fluid Mech.*, *637*, 387–424.
Fuchs, M., and C. B. Tanner (1967), Evaporation from a drying soil, *J. Appl. Meteorol.*, *6*, 852–857.
Gao, W., R. H. Shaw, K. T. Paw (1989), Observation of organized structure in turbulent flow within and above a forest canopy, *Boundary Layer Meteorol.*, *74*, 349–377.
Gillespie, A., S. Rokugawa, T. Matsunaga, J. S. Cothern, S. Hook, and A. B. Kahle (1998), A temperature and emissivity separation algorithm for advanced spaceborne thermal emission and reflection radiometer (ASTER) images, *IEEE Trans. Geosci. Remote Sens.*, *36*(4), 1113–1126.
Goffe, W. L., G. D. Ferrier, and J. Rogers (1994), Global optimization of statistical functions with simulated annealing, *J. Econom.*, *60*, 65–100.
Goulden, M. L., J. W. Munger, S. M. Fan, B. C. Daube, and S. C. Wofsy (1996), Measurements of carbon storage by long-term eddy correlation: Methods and a critical assessment of accuracy, *Global Change Biol.*, *2*, 169–182.
Graefe, J. (2004), Roughness layer corrections with emphasis on SVAT model applications, *Agric. For. Meteorol.*, *124*, 237–251.
Guzinski, R., M. C. Anderson, W. P. Kustas, H. Nieto, and I. Sandholt (2013), Using a thermal-based two source energy balance model with time-differencing to estimate surface energy fluxes with day-night MODIS observations, *Hydrol. Earth Syst. Sci.*, *17*, 2809–2825.
Harman, I. N., and J. J. Finnigan (2007), A simple unified theory for flow in the canopy and roughness sublayer, *Boundary Layer Meteorol.*,*123*, 339–363.
Harman, I. N., and J. J. Finnigan (2008), Scalar concentration profiles in the canopy and roughness sublayer, *Boundary Layer Meteorol.*,*129*, 323–351.
Haverd, V., M. Böhm, and M. R. Raupach (2010), The effect of source distribution on bulk scalar transfer between a rough land surface and the atmosphere, *Boundary Layer Meteorol.*, *135*, 351–368.
Hongyan, C. Jiayi, F. Hu, and Z. Qingcun (2004), The coherent structure of wáter wapor transfer in the unstable atmospheric surface layer, *Boundary Layer Meteorol.*, *111*, 534–552.
Jacob, F., F. Petitcolin, T. Schmugge, E. Vermote, K. Ogawa, and A. French (2004), Comparison of land surface emissivity and radiometric temperature derived from MODIS and ASTER sensors, *Remote Sens. Environ.*, *90*, 137–152.
Jiménez-Munõz, J. C., and J. A. Sobrino (2007), Feasibility of retrieving land-surface temperature from ASTER TIR bands using two-channel algorithms: A case study of agricultural areas, *IEEE Trans. Geosci. Remote Sens. Lett.*, *4*(1), 60–64.
Kalma, J. D., T. R. McVicar, and M. F. McCabe (2008), Estimating land surface evaporation: A review of methods using remotely sensed surface temperature data, *Surv. Geophys.*, *29*, 421–469.
Katul, G. G., C-I. Hsieh, R. Oren, D. Ellsworth, and N. Philips (1996), Latent and sensible heat flux predictions from a uniform pine forest using surface renewal and flux variance methods, *Boundary Layer Meteorol.*, *80*, 249–282.
Kustas, W. P., B. J. Choudhury, M. S. Moran, R. J. Reginato, R. D. Jackson, L. W. Gay, and H. L. Weaver (1989), Determination of sensible heat flux over sparse canopy using thermal infrared data, *Agric. For. Meteorol.*, *46*, 197–216.
Liu, Y., Y. Yamaguchi, and C. Ke (2007), Reducing the discrepancy between ASTER and MODIS land surface temperature products, *Sensors*, *7*, 3043–3057.
Mengistu, M. G., and M. J. Savage (2010), Open water evaporation estimation for a small shallow reservoir in winter using surface renewal, *J. Hydrol.*, *380*(1), 27–35.
Metropolis, W., A. Rosenbluth, A. Teller, and E. Teller (1953), Equation of state calculation by fast computing machines, *J. Chem. Phys.*, *21*, 1087–1092.
Mölder, M., A. Grelle, A. Lindroth, and S. Halldin (1999), Flux profile relationships over a boreal forest roughness sublayer corrections, *Agric. For. Meteorol.*, *98*(99), 645–658.
Moratiel, R., and A. Martínez-Cob (2012), Evapotranspiration of grapevine trained to a gable trellis system under netting and black plastic mulching, *Irrig. Sci.*, *30*(3), 167–178.

Morillas, L., M. García, H. Nieto, L. Villagarcia, I. Sandholt, M. P. Gonzalez-Dugo, P. J. Zarco-Tejada, and F. Domingo (2013), Using radiometric surface temperature for surface energy flux estimation in Mediterranean drylands from a two-source perspective, *Remote Sens. Environ.*, *136*, 234–246.

Mu, Q., M. Zhao, J. S. Kimball, N. G. McDowell, and S. W. Running (2013), A remotely sensed global terrestrial drought severity index, *Bull. Am. Meteorol. Soc.*, *94*, 83–98.

Nardino, M., F. Pernice, F. Rossi, T. Georgiadis, O. Facini, A. Motisi, and A. Drago (2013), Annual and monthly carbon balance in an intensively managed Mediterranean olive orchard, *Photosynthetica*, *51*(1), 63–74.

Norman, J. M., and F. Becker (1995), Terminology in thermal infrared remote sensing of natural surfaces, *Remote Sens. Rev.*, *12*(3-4), 159–173.

Norman, J. M., W. P. Kustas, and K. S. Humes (1995), Source approach for estimating soil and vegetation energy fluxes in observations directional radiometric surface temperature, *Agric. For. Meteorol.*, *77*, 263–293.

Norman, J. M., W. P. Kustas, J. H. Prueger, and G. R. Diak (2000), Surface flux estimation using radiometric temperature: A dual-temperature-difference method to minimize measurement errors, *Water Resour. Res.*, *36*(8), 2263–2274.

Ogawa, K., T. Schmugge, F. Jacob, and A. French (2002), Estimation of broadband land surface emissivity from multi-spectral thermal infrared remote sensing, *Agronomie*, *22*(6), 695–696.

Paw, U. K. T., Y. Brunet, S. Collineau, R. H. Shaw, T. Maitani, J. Qiu, and L. Hipps (1992), On coherent structures in turbulence within and above agricultural plant canopies, *Agric. For. Meteorol.*, *61*, 55–68.

Paw, U. K. T, J. Qiu, H-B. Su, T. Watanabe, and Y. Brunet (1995), Surface renewal analysis: A new method to obtain scalar fluxes without velocity data, *Agric. For. Meteorol.*, *74*, 119–137.

Paw, U. K. T., R. L. Snyder, D. Spano, and H.-B. Su (2005), Surface renewal estimates of scalar exchange, in *Micrometeorology in Agricultural Systems, Agron. Monogr. 47*, edited by J. L. Hatfield and J. M. Baker, pp. 455–483, ASA-CSSA-SSSA, Madison, Wis.

Priestley, C. H. B., and R. J. Taylor (1972), On the assessment of surface heat flux and evaporation using large-scale parameters, *Mon. Weather Rev.*, *100*, 81–92.

Qiu, J., U. K. T. Paw, and R. H. Shaw (1995), Pseudo-Wavelet analysis of turbulence patterns in three vegetations layers, *Boundary Layer Meteorol.*, *72*, 177–204.

Raupach, M. R. (1994), Simplified expressions for vegetation roughness length and zero-plane displacement as functions of canopy height and area index, *Boundary Layer Meteorol.*, *71*(1-2), 211–216.

Raupach, M. R., J. J. Finnigan, and Y. Brunet (1996), Coherent eddies in vegetation canopies: The mixing-layer analogy, *Boundary Layer Meteorol.*, *78*, 351–382.

Sakai, R., D. Fitzjarrald, and K. E. Moore (2001), Importance of low-frequency contributions to eddy fluxes observed over rough surfaces, *J. Applied Meteorol.*, *40*, 2178–2192.

Schmugge, T. J. (2006), Estimation of surface temperature and surface emissivity, *Encycl. Hydrol. Sci.*, *5*, 52.

Schmugge, T. J., A. French, J. Ritchie, and A. Rango (2001), Estimation of surface emissivity for arid lands, in *Proceedings of a Symposium on Remote Sensing and Hydrology 2000*, *IAHS Publ.*, *267*, 168–174.

Shapland, T. M, A. J. McElrone, R. L. Snyder, and K. T. Paw (2012a), Structure function analysis of two-scale scalar ramps. Part I: Theory and modelling, *Boundary Layer Meteorol.*, *145*, 5–25.

Shapland, T. M, A. J. McElrone, R. L. Snyder, and K. T. Paw (2012b), Structure function analysis of two-scale scalar ramps. Part II: Ramp characteristics and surface renewal flux estimation, *Boundary Layer Meteorol.*, *145*, 27–44.

Shaw, R. H., K T. Paw, and W. Gao (1989), Detection of temperature ramps and flow structures at a deciduous forest site, *Agric. For. Meteorol.*, *47*, 123–138.

Shaw, R. H., Y. Brunet, J. J. Finnigan, and M. R. Raupach (1995), A wind tunnel study of air flow in waving wheat: Two-point velocity statistics, *Boundary Layer Meteorol.*, *76*, 349–376.

Snyder, R. L., D. Spano, and K. T. Paw (1996), Surface renewal analysis for sensible and latent heat flux density, *Boundary Layer Meteorol.*, *77*, 249–266.

Su, Z. (2012), The Surface Energy Balance System (SEBS) for estimation of turbulent heat fluxes, *Hydrol. Earth Syst. Sci.*, *6* (1), 85–99.

Suvočarev, K., T. M Shapland, R. L. Snyder, and A. Martínez-Cob (2014), Surface renewal performance to independently estimate sensible and latent heat fluxes in heterogeneous crop surfaces, *J. Hydrol.*, *509*, 83–93.

Teixeira, A. H. C., W. G. M. Bastiaanssen, M. S. B. Moura, J. M. Soares, M. D. Ahmad, M. G. Bos (2008), Energy and water balance measurements for water productivity analysis in irrigated mango trees, Northeast Brazil, *Agric. For. Meteorol.*, *148*, 1527–1537.

Twine, T. E., W. P. Kustas, J. M. Norman, D. R. Cook, P. R. Houser, T. P. Meyers, J. H. Prueger, P. J. Starks, and M. L. Wesely (2000), Correcting eddy-covariance flux underestimates over a grassland, *Agric. For. Meteorol.*, *103*, 279–300.

Valor, E., and V. Caselles (2005), Validation of the vegetation cover method for land surface emissivity estimation, in *Recent Research developments in Thermal Remote Sensing*, pp. 1–20, Res. Signpost, Kerala, India.

Van Atta, C. W. (1977), Effect of coherent structures on structure functions of temperature in the atmospheric boundary layer, *Arch. Mech.*, *29*, 161–171.

Wan, Z., and J. Dozier (1996), A generalized split-window algorithm for retrieving land-surface temperature from space, *IEEE Trans. Geosci. Remote Sens.*, *34*(4), 892–905.

Wilson, K., et al. (2002), Energy balance closure at FLUXNET sites, *Agric. For. Meteorol.*, *113*, 223–143.